

Supplementary information:
**Sign reversal of magnetoresistance in a perovskite nickelate by
electron doping**

Koushik Ramadoss¹, Nirajan Mandal^{2,3}, Xia Dai⁴, Zhong Wan², You Zhou⁵, Leonid
Rokhinson^{2,3,6}, Yong P. Chen^{2,3,6}, Jiangpin Hu² and Shriram Ramanathan¹

¹*School of Materials Engineering, Purdue University, West Lafayette, IN 47907*

²*Department of Physics and Astronomy,
Purdue University, West Lafayette, IN 47907*

³*Birck Nanotechnology Center, Purdue University, West Lafayette, IN 47907*

⁴*Institute of Physics, Chinese Academy of Sciences,
P.O.Box 603, Beijing 100190, China*

⁵*School of Engineering and Applied Sciences,
Harvard University, Cambridge, MA 02138 and*

⁶*School of Electrical and Computer Engineering,
Purdue University, West Lafayette, IN 47907*

I. FIRST PRINCIPLES CALCULATIONS OF RAMAN SPECTRUM

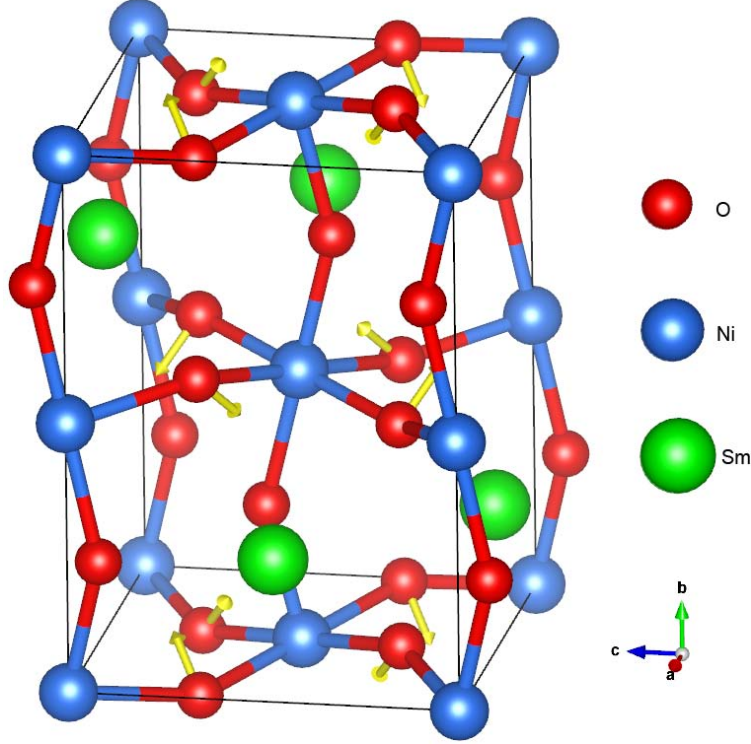


Figure S1: Atom displacements of the phonon mode at 444.9 cm^{-1} .

The first-principles calculations employ the projector augmented wave (PAW) method encoded in Vienna ab initio simulation package (VASP) [1–3] and generalized-gradient approximation (GGA) [4] for the exchange correlation functions is used. The cutoff energy is set to be 500 eV. The number of the k points is $5 \times 5 \times 5$ for the $2 \times 1 \times 2$ supercell. Forces are minimized to less than $0.01 \text{ eV}/\text{\AA}^\circ$ when we relax the lattice. Real-space force constants of supercells are calculated in the density-functional perturbation theory (DFPT) [5], and phonon frequencies are calculated from the force constants using the PHONOPY code [6]. The lattice parameters and the internal atomic positions of SNO in the monoclinic $P2_1/n$ space group are fully relaxed and the initial atomic positions are from the isostructural compound YNiO_3 [7]. The resulting lattice parameters have little difference with those in the orthorhombic phase. Our calculations of phonon dispersions show that there are no imaginary frequencies throughout the whole Brillouin zone, which confirms the dynamical structural stability. For pristine SNO, we have calculated 60 phonon modes, consisting of 24 Raman active modes, 33 IR active modes and 3 acoustic modes. Among the 24 Raman

active modes, 8 modes are observed in experiment that are in good agreement with calculations. The modes with smaller frequencies are mainly contributed from the movements of heavy Sm atoms and those with larger frequencies are mainly attributed to the movements of O atoms. Fig. S1 shows the atomic displacements corresponding to the phonon mode at 444.9 cm^{-1} . Our calculations show that the mode is mainly contributed from the movements of O atoms in the $8d$ Wyckoff positions. When doped with H, the protons are mostly likely to bond with O atoms, thus the mode will be greatly affected in HSNO. It is consistent with the experimental observation that the mode is absent in HSNO.

II. MAGNETORESISTANCE MODELS

In this section, we discuss various literature models of magnetoresistance phenomena as applied to diffusive and localized regimes in correlated oxide systems. In the case of SNO which shows strong localization, the magnetoresistance is dictated by spin correlations, we present a comparison of our data to other models for the sake of completeness.

A. Weak Localization:

The phenomenon of weak localization (WL) leads to a negative MR due to the destruction of quantum interference of electrons by an applied magnetic field. In two dimensions, the quantum correction to conductivity is given by [8]

$$\Delta\sigma_{2D-WL} = \frac{e^2}{\pi h} \left[\Psi \left(\frac{1}{2} + \frac{H_\phi}{H} \right) - \Psi \left(\frac{1}{2} + \frac{H_{tr}}{H} \right) - \ln \frac{H_\phi}{H_{tr}} \right] \quad (1)$$

where $H_\phi = \frac{\hbar}{4eL_\phi^2}$ is the phase breaking field and H_{tr} is the transport field. Here L_ϕ is the phase breaking length. The 2D WL model can be used only when the film thickness $d < L_\phi$. Thus one can model the magnetoconductance (MC) in SNO by the following equation:

$$\Delta\sigma = -A_1 \frac{H^2}{H^2 + H_e^2} + \Delta\sigma_{2D-WL} \quad (2)$$

where A_1 is the saturation value, H_e is the characteristic field for spin alignment.

The MC for SNO along with the fits (with Eqn. 2) are shown in Fig. S2a. The phase coherence length extracted from the fits (Fig. S2b) is less than the thickness of the film ($L_\phi < d$). This rules out the use of this model to analyze our data.

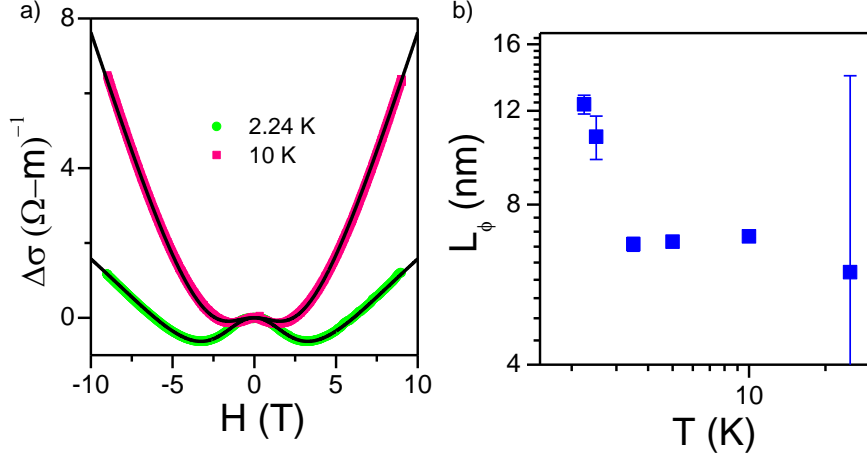


Figure S2: a) $\Delta\sigma$ vs H for SNO film at two different temperature. The black lines are fits to the data according to Eqn. 2 b) Plot of L_ϕ vs T for SNO.

For thicker films, the 3D WL model proposed by Kawabatta [9] is used and correction to conductivity is given by

$$\Delta\sigma_{3D-WL} = \frac{e^2}{2\pi^2\hbar} \left(\frac{eH}{\hbar}\right)^{1/2} f_3\left(\frac{H}{H_{in}}\right) \quad (3)$$

$$f_3(x) = \begin{cases} 0.605 & x \gg 1 \\ \frac{x^{3/2}}{48} & x \ll 1 \end{cases}$$

where $H_{in} = \frac{\hbar}{4eL_{in}^2}$ is the field associated with inelastic scattering with L_{in} being the inelastic scattering length that breaks the phase coherence of the electrons. Using this model, MC in SNO is given as

$$\Delta\sigma = -A_1 \frac{H^2}{H^2 + H_e^2} + \Delta\sigma_{3D-WL} \quad (4)$$

Fig. S3a shows the fits for $\Delta\sigma$ as a function of magnetic field at different temperatures along with fits to Eqn. 2. Through fitting $\Delta\sigma$, we find that the fit parameter L_{in} is smaller compared to the localization length ($\xi = 37$ nm) and moreover L_{in} displays a non-monotonic behavior as a function of temperature. It is well known that L_{in} in thin films exhibits a T^{-p} behavior signifying the dominant scattering mechanism due to phonons ($p = 2$) or electron-electron interactions ($p = 3/2$) [10]. Thus one can conclude the weak localization is not the right mechanism to describe the magnetotransport properties of SNO.

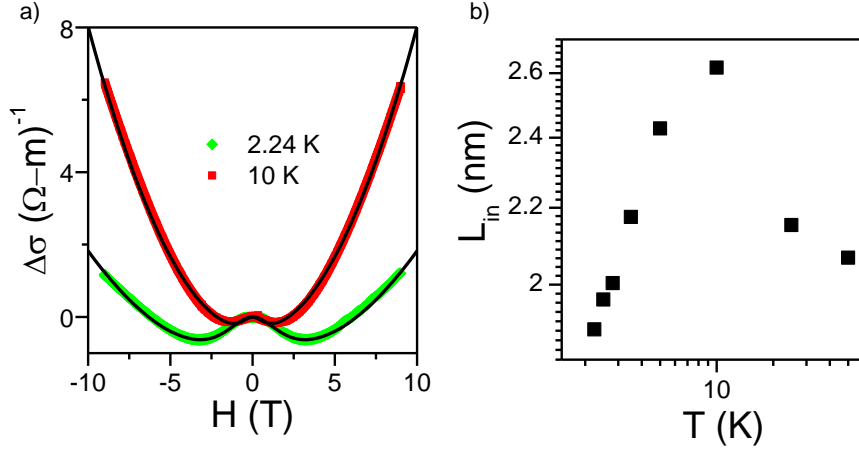


Figure S3: a) $\Delta\sigma$ vs H for SNO film at two different temperature. The black lines are fits to the data according to Eqn. 4 b) Plot of L_{in} vs T for SNO.

B. Forward Interference model:

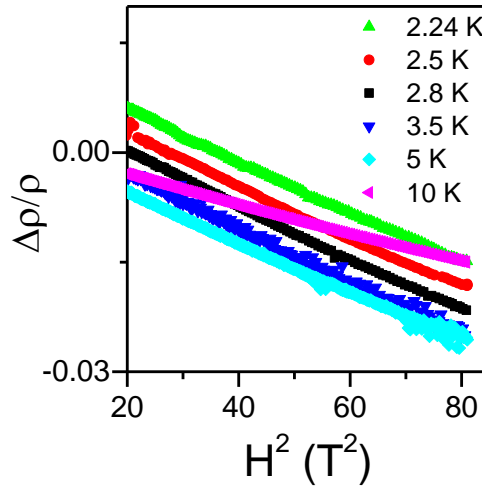


Figure S4: $\Delta\rho/\rho$ vs H^2 for SNO film at various temperatures.

Several insulating systems showing localization behavior, display a negative MR due to the forward interference among the various paths between the hopping sites. According to this model, the MR decreases linearly with field and saturates at high field. The MR is given by [11–13]

$$\frac{\Delta\rho}{\rho} = -c_{sat} \frac{H}{H_{sat}} \quad (5)$$

where c_{sat} is the saturation value and H_{sat} is the characteristic field beyond which MR saturates and expressed as $H_{sat} \approx 0.7 (h/e) (8/3)^{3/2} (1/\xi^2) (T/T_{Mott})^{3/8}$. The forward interference model predicts the saturation field to be $H_{sat} \sim 1$ T at 10 K. As shown in Fig. S4, MR shows a quadratic dependence with field upto 9 T with no sign of saturation. Thus this model cannot describe the MR obtained for SNO.

C. Two Band model:

Hedgcock *et. al* [14] had proposed that in heavily doped semiconductors, the conduction band electrons move between two bands of different mobilities which gives rise to a negative magnetoresistance at low fields. According to this two band model, the magnetoresistance should vary linearly with field. But SNO thin films show a quadratic dependence over a large field range which rules out the use of two band model for our system.

III. OXYGEN DEFICIENT SNO

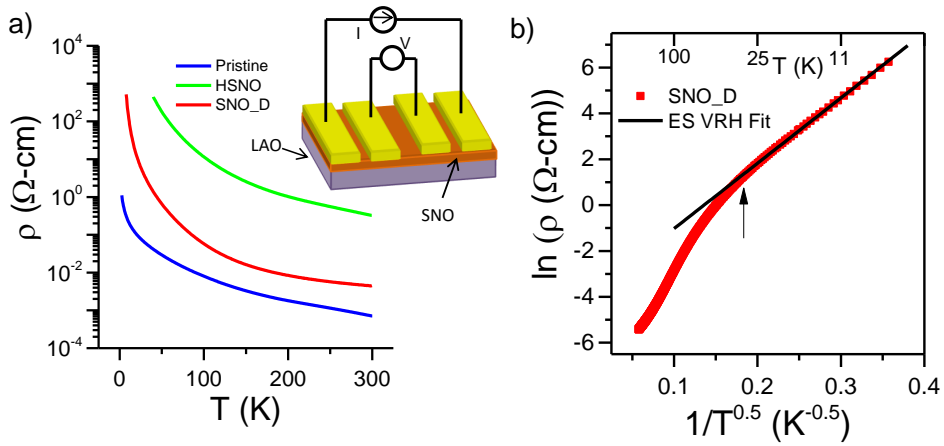


Figure S5: a) Temperature dependence of resistance at $H = 0$ T for SNO, SNO_D and H-SNO showing an insulating behavior. Inset shows a schematic of the electrical measurement. The metal contacts to the sample are shown in yellow. b) Plot of $\ln(\rho)$ vs $T^{-1/2}$ for SNO_D. Black line is linear fit indicating ES VRH. The upward pointing arrow indicates the crossover regime from ES VRH to activated transport.

In this section, we detail transport measurements performed on oxygen deficient SNO

to show its unique behaviour that is completely different from that of pristine and electron doped SNO films.

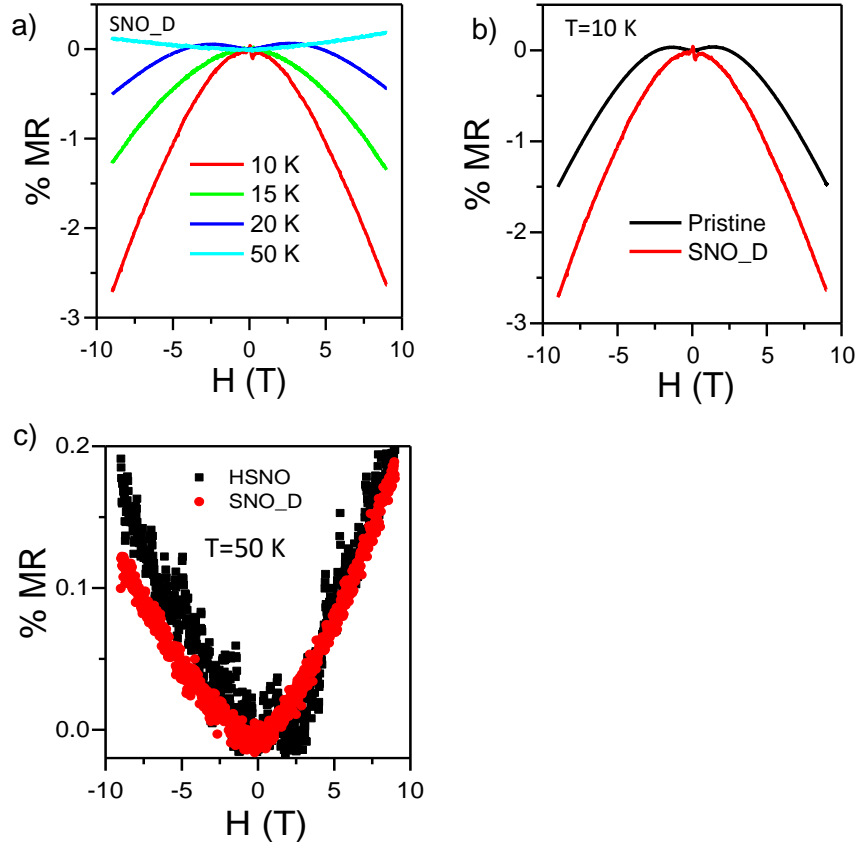


Figure S6: a) Magnetoresistance (in %) vs H for SNO_D film at various temperatures. b) Comparison of magnetoresistance (in %) vs H for SNO and SNO_D films at $T = 10$ K. c) Comparison of magnetoresistance (in %) vs H for SNO_D and HSNO films at $T = 50$ K.

Oxygen deficient SNO films (referred to as SNO_D) were prepared by annealing pristine SNO films for 3 hours at 300°C under low oxygen partial pressure (10^{-24} Atm) in a solid state buffer apparatus. The ρ vs T characteristics of SNO_D is shown in Fig. S5a and compared with that of pristine and electron doped films. SNO_D shows larger resistivity compared to SNO films due to both greater amount of disorder due to oxygen vacancies and charge compensation leading to electron doping of the Ni^{3+} site [15]. A detailed analysis shows that SNO_D films exhibit ES VRH behavior below 30 K with $T_{ES} = 812$ K and assuming a $\epsilon_r \sim 10$ (intermediate value between SNO and HSNO) for oxygen deficient SNO, $\xi \sim 5.7$ nm (Fig. S5b) from a similar approach to that described in the main manuscript. We have

also measured the MR of SNO_D sample at different temperatures. The MR of SNO_D (Fig. S6a) shows a crossover from negative MR to positive as a function of temperature unlike SNO and HSNO. At the lowest temperature $T = 10$ K, the MR is similar to pristine SNO (Fig. S6b) whereas at $T = 50$ K the MR resembles that of HNSO (Fig. S6c). This change in sign of MR from negative to positive directly correlates to change of hopping mechanism namely ES VRH at low temperature ($T \lesssim 35$ K) to activated transport at high temperatures. Similar crossover in MR with temperature has also been observed in Si delta doped GaAs quantum wells [16], correlated iridates like Sr_2IrO_4 [17] and attributed to the change in transport mechanism.

These experiments on SNO_D conclusively show that sign reversal in MR between pristine SNO and HSNO is not simply due to temperature effects and there is rich physics in each set of samples.

-
- [1] G. Kresse and J. Hafner, Phys. Rev. B **47**, 558 (1993).
 - [2] G. Kresse and J. Furthmüller, Comput. Mater. Sci. **6**, 15 (1996).
 - [3] G. Kresse and J. Furthmüller, Phys. Rev. B **54**, 11169 (1996).
 - [4] J. P. Perdew, K. Burke, and M. Ernzerhof, Phys. Rev. Lett. **77**, 3865 (1996).
 - [5] S. Baroni, P. Giannozzi, and A. Testa, Phys. Rev. Lett. **58**, 1861 (1987).
 - [6] A. Togo, F. Oba, and I. Tanaka, Phys. Rev. B **78**, 134106 (2008).
 - [7] J. A. Alonso, M. J. Martinez-Lope, M. T. Casais, M. A. Aranda, and M. T. Fernandez-Diaz, J. Am. Chem. Soc. **121**, 4754 (1999).
 - [8] S. Hikami, A. I. Larkin, and Y. Nagaoka, Prog. Theor. Phys. **63**, 707 (1980).
 - [9] A. Kawabata, J. Phys. Soc. Jpn. **49**, 628 (1980).
 - [10] G. Bergmann, Phys. Rep. **107**, 1 (1984).
 - [11] B. Shklovskii, Sov. Phys. Semicond. **17**, 1311 (1983).
 - [12] B. I. Shklovskii and A. L. Efros, *Electronic properties of Doped Semiconductors* (Springer-Verlag, 1984).
 - [13] R. Rosenbaum, T. Murphy, E. Palm, S. Hannahs, and B. Brandt, Phys. Rev. B **63**, 094426 (2001).
 - [14] F. Hedgcock and T. Raudorf, Solid State Commun. **8**, 1819 (1970).

- [15] L. Wang, S. Dash, L. Chang, L. You, Y. Feng, X. He, K. Jin, Y. Zhou, H. G. Ong, P. Ren, et al., *ACS Appl. Mater. Interfaces* **8**, 9769 (2016).
- [16] S.-T. Lo, K. Y. Chen, Y.-C. Su, C.-T. Liang, Y. Chang, G.-H. Kim, J.-Y. Wu, and S.-D. Lin, *Solid State Commun.* **150**, 1104 (2010).
- [17] J. Ravichandran, C. R. Serrao, D. Efetov, D. Yi, Y. Oh, S.-W. Cheong, R. Ramesh, and P. Kim, arXiv preprint arXiv:1312.7015 (2013).